Conformational Changes in the Cytoplasmic Domain of Human Anion Exchanger 1 Revealed by Luminescence Resonance Energy Transfer†

Prithwish Pal,* Brian E. Holmberg, and Philip A. Knauf

Department of Biochemistry and Biophysics, University of Rochester Medical Center, 601 Elmwood Avenue, Box 712, Rochester, New York 14620

Received April 14, 2005; Revised Manuscript Received August 15, 2005

ABSTRACT: The cytoplasmic domain of the human erythrocyte anion exchanger 1 (cdAE1) serves as a center of organization for the red blood cell cytoskeleton as well as several metabolic enzymes and hemoglobin. The protein is known to undergo a reversible pH-dependent conformational change characterized by a 2-fold change in the intrinsic fluorescence and an 11 Å change in the Stokes radius. While the exact changes in the molecular structure are unknown, on the basis of the crystal structure of the protein at pH 4.8 and site-directed mutagenesis studies, Zhou and Low (*19*) have proposed that the peripheral protein binding (PPB) domain of cdAE1 moves away from the dimerization domain in response to increasing alkalinity. To test this hypothesis, we have applied luminescence resonance energy transfer (LRET) to measure the intermonomer distance between donor and acceptor probes at the Cys^{201} site (located in the PPB domain) within the cdAE1 dimer. This distance was found to increase as the pH is increased from 5 to 10, in recombinant forms of both the wild type and a mutant (C317S) of cdAE1. Furthermore, LRET measurements in red blood cell inside-out vesicles indicate that when cdAE1 is linked to the membrane, the intermonomer distance is larger at pH 5, compared to that of the purified cdAE1 segments, and exhibits a different pH-dependent behavior. An increase in the distance was also observed on binding of a metabolic enzyme, glyceraldehyde-3-phosphate dehydrogenase, to cdAE1. These data provide the first demonstration of a defined change in the molecular structure of cdAE1, and also indicate that the structure under physiological conditions is different from the crystal structure determined at low pH.

The human erythrocyte anion exchanger 1 (hAE1[1] or band 3) is the most abundant protein in the red blood cell membrane, comprising 50% of the total integral membrane proteins (*1*). The 911-amino acid protein consists of two distinct structural and functional domains: (a) a 43 kDa N-terminal cytoplasmic domain (cdAE1 or cdb3) that includes residues 1−404 that serves as an anchor for the red blood cell cytoskeleton and other proteins (*2*) and (b) a 55 kDa C-terminal membrane-spanning domain (mdAE1 or mdb3) that is responsible for the exchange of chloride and bicarbonate across the membrane (*1*). Each domain retains its structure and is capable of functioning independently either after enzymatic cleavage or when expressed individually as recombinant proteins in heterologous systems. A major portion of cdAE1 (amino acids 1−379) has been expressed in *Escherichia coli* and its crystal structure at pH 4.8 determined to 2.6 Å resolution (Figure 1) (*3*). This crystal structure, as well as other biochemical evidence, indicates that full-length hAE1 is a homodimer in the membrane and that cdAE1 exists as a dimer in solution as well.

FIGURE 1: PPB and dimerization domains in the cdAE1 dimer. The crystal structure of cdAE1 at 2.6 Å resolution at pH 4.8 is shown. The PPB domains (see text) of both monomers are colored magenta, while the dimerization domains are colored yellow or cyan for each monomer. The red spheres indicate the location of Cys^{201} in each monomer. The distance between these is called the inter-Cys^{201} or intermonomer distance. The thick blue arrow points to Gly^{305} (violet spheres), around which the conformational change proposed by Zhou and Low (*19*) is supposed to occur. The Trp^{105} (green) and Asp^{316} (dark blue) residues, which form a putative hydrogen bond, are also shown. The image was created with PyMol (http://pymol.sourceforge.net/) using the coordinates of PDB entry 1HYN (*3*).

† This work was supported by NIH (NIDDK) Grant R01 DK27495.

* To whom correspondence should be addressed. Present address: Department of Pharmacology, University of North Carolina, CB# 7365, Rm 1131, Mary Ellen Jones Building, Chapel Hill, NC 27599. Fax: (919) 966-5640. Phone: (919) 843-2752. E-mail: ppal@med.unc.edu.

[1] Abbreviations: hAE1, human anion exchanger 1; cdAE1, cytoplasmic domain of hAE1; mdAE1, membrane domain of hAE1; LRET, luminescence resonance energy transfer; cs124-DTPA-EMCH, diethylenetriaminepentaacetate-carbostyril 124-maleimidocaproic hydrazide; FM, fluorescein 5-maleimide; TbM, terbium maleimide; G3PDH, glyceraldehyde-3-phosphate dehydrogenase; PMSF, phenylmethanesulfonyl fluoride; DTT, dithiothreitol; IOV, inside-out vesicles.

10.1021/bi0506831 CCC: $30.25
Published on Web 09/27/2005

A variety of proteins are known to interact with cdAE1. These include the cytoskeletal proteins ankyrin (*4*, *5*), protein 4.1 (*6*), and protein 4.2 (*7*); glycolytic enzymes such as aldolase (*8*), glyceraldehyde-3-phosphate dehydrogenase (*9*, *10*), and phosphofructokinase (*11*); and hemoglobin (*12*), hemichromes (*13*), and a tyrosine kinase (*14*). These interactions serve major physiological roles, including membrane stability and flexibility (*15*−*17*), regulation of glucose metabolism (*9*), and control of cell life span (*18*). Mutations mapped to cdAE1 have been shown to alter these functions.

An interesting property of cdAE1 is its ability to undergo a reversible pH-dependent conformational change. As the pH is increased from 6 to 10, the Stokes radius of the protein increases from 52 to 63 Å (*19*), the intrinsic fluorescence more than doubles, the thermal stability decreases by ∼15 °C, and both the extent of protein segmental motion (*20*) and the protein axial ratio increase significantly (*2*, *19*, *21*). Extensive characterization of this pH-dependent conformational change indicates that it involves three states with p*K*'s for conversion between states of 7.2 and 9.2 (*21*). Because of these conformational changes, the structure of cdAE1 at physiological pH could be different from the crystal structure of the protein at pH 4.8. Additionally, it has been observed that binding of peripheral proteins depends on the conformational state of cdAE1. For example, ankyrin binds more avidly to the low-pH conformation (*22*), and hemoglobin binding is also affected by pH (*12*). Therefore, these conformational changes are physiologically relevant, and it is important to understand the nature of the structural changes.

From the crystal structure, it is possible to predict which regions of cdAE1 might be flexible enough to undergo pH-induced movements. The structure of cdAE1 indicates that it forms a tight symmetrical dimer, with a shared dimerization domain and a flanking peripheral protein binding (PPB) domain (Figure 1). Since the conformational change occurs without a significant change in the secondary structure of the protein, Zhou and Low (*19*) proposed that the observed biophysical changes are caused by movement of the PPB domain away from the dimerization domain by rotating around a hinge at Gly^{305} (shown with a blue arrow in Figure 1). This "domain rotation hypothesis" was supported by studies involving the mutation of two residues, Trp^{105} and Asp^{316}, involved in a prominent hydrogen bond between the PPB and the dimerization domains.

To test this hypothesis and to obtain information about the actual changes in molecular location during the conformational change, resonance energy transfer was used to measure the intermonomer distance between fluorescent labels at the Cys^{201} site in each monomer, within the cdAE1 homodimer (Figure 1). Cys^{201} has been observed to be more maleimide-reactive (*23*) than the only other cysteine residue in cdAE1, Cys^{317}. According to the domain rotation hypothesis, an increase in the intermonomer distance between Cys^{201} residues is predicted with an increase in pH.

Labeling identical residues in each monomer of a homodimer generates a heterogeneous dimer population consisting of dimers labeled with two donors, two acceptors, or donor−acceptor pairs. With conventional energy transfer using steady state or lifetime measurements, contributions to the fluorescence intensity from direct excitation of the acceptors or emission from donors that do not have an adjacent acceptor reduce the signal-to-noise ratio and greatly complicate the interpretation of changes in donor or acceptor fluorescence. These problems can be overcome by the novel energy transfer technique called lanthanide (or luminescence) resonance energy transfer (LRET) as described in the Results.

In this study, the intermonomer distance between Cys^{201} (termed the inter-Cys^{201} distance) is measured over a range of pH's (5−10) in isolated cdAE1 dimers in the form of purified wild-type and C317S (with the cysteine at position 317 mutated to a serine) recombinant proteins and compared with the distance between the sulfur atoms of Cys^{201} in the crystal structure (42 Å). Since some investigators have reported a communication between the membrane and cytoplasmic domains of hAE1, the inter-Cys^{201} distance is also measured in intact hAE1 in its native environment, using KI-stripped inside-out vesicles (IOVs) of RBCs. Moreover, to investigate more physiological causes of these structural changes, the effects of binding of glyceraldehyde-3-phosphate dehydrogenase, as well as bicarbonate and chloride ions, on the conformation of cdAE1 were also measured.

EXPERIMENTAL PROCEDURES

Materials. The terbium chelate maleimide donor label, diethylenetriaminepentaacetate-carbostyril 124-maleimidocaproic hydrazide (cs124-DTPA-EMCH), was synthesized according to published protocols (*24*) by T. Ryder and R. Boeckman (Department of Chemistry, University of Rochester, Rochester, NY). Fluorescein maleimide (FM) was purchased from Molecular Probes (Eugene, OR). Terbium chloride, glyceraldehyde-3-phosphate dehydrogenase (G3PDH), phenylmethanesulfonyl fluoride (PMSF), and dithiothreitol (DTT) were purchased from Sigma-Aldrich (St. Louis, MO).

Preparation of IOVs and Expression of Recombinant cdAE1. Washing of blood, obtained with informed consent from apparently healthy individuals, hypotonic lysis, spectrin removal, and preparation of inside-out vesicles (IOVs) were performed according to published protocols (*25*, *26*). pT7-7 expression vectors containing the wild-type cytoplasmic domain of hAE1 (residues 1−379) and a mutant (C317S) were kindly provided by Philip Low (Purdue University, West Lafayette, IN). Both cDNAs are engineered with a C-terminal $(His)_6$ tag (*4*). The proteins were expressed in *E. coli* BL21(DE3) pLysS cells by isopropyl beta-D-thiogalactopyranoside (IPTG) induction for 3 h at 37 °C. Cells were spun down and lysed by Bugbuster reagent (Novagen, Madison, WI), supplemented with 100 μM PMSF. Cell lysates were incubated with Ni−NTA agarose (Novagen) beads for 1 h at 4 °C, which were then loaded into an empty column. Columns were washed with a buffer containing 300 mM sodium chloride, 50 mM sodium phosphate, and 10 mM imidazole (pH 8), and the cdAE1 proteins were eluted with the same buffer but containing 250 mM imidazole.

Labeling. The terbium chelator, cs124-DTPA-EMCH, was incubated with a 0.9:1 molar ratio of $TbCl_3$ for 30 min on ice to obtain the terbium chelate label (TbM). Wild-type and C317S cdAE1 proteins (1 mg/mL) or IOVs (1 mg/mL cdAE1, assuming 50% of the total proteins are hAE1) were labeled in a 135 mM NaCl, 10 mM phosphate buffer (pH 7.4) with a 10-fold molar excess of either TbM (donor only) or an equimolar mixture (also 10-fold excess each) of TbM and FM (donor−acceptor) and incubated either at room

temperature for 4 h or at 4 °C overnight. Reactions were stopped with 1 mM DTT and unreacted dyes separated from the pure proteins by being passed through a Sephadex G-25 column (CS100 from Princeton Separations, Adelphia, NJ) pre-equilibrated with the titration buffer {50 mM sodium phosphate, 50 mM sodium borate, and 70 mM NaCl (pH 8) [TB50(8)]}. IOVs were washed extensively (five to six times) by centrifugation at 40000*g* for 40 min with TB50(8) to remove the unreacted dyes.

Luminescence Lifetime and Intrinsic Fluorescence Measurements. The luminescence of terbium or sensitized acceptor decay was measured using the 337 nm excitation wavelength of a pulsed N_2 laser (model 3370, Laser Pulse Inc.) operating at 30 Hz. Emission was detected at right angles, after collimating with a lens and passing through an appropriate interference filter (see below), by an ultra-high-speed single photon counting PMT (P10PC from Electron Tubes). The output from the PMT was binned at 2 μs resolution by a multichannel scalar card (MCS-pci from ORTEC) and averaged over the total number of laser shots (500−1500) to provide the luminescence decay curves. A 490 ± 5 nm interference filter was used for observing donor luminescence and a 520 ± 5 nm filter (Omega Filters, Brattleboro, VT) for sensitized acceptor emission. Labeled proteins or IOVs in TB50(8) prepared as described above were diluted into TB50 preadjusted to the desired pH (or other buffers where indicated) for luminescence measurements. To guard against inner filter effects or intermolecular energy transfer, decay curves were obtained for different dilutions of the protein (1−50 μg/mL). We did not find any differences in energy transfer at various concentrations. For determining the effects of G3PDH binding, a 5-fold molar excess of the enzyme was added to the diluted protein in 10 mM sodium phosphate (pH 6.5). Control experiments were conducted with the addition of the buffer only. In the case of the G3PDH binding experiments, Oregon Green maleimide (Molecular Probes) was used as an acceptor instead of FM. The spectral properties (absorbance and emission profiles) of Oregon Green are similar to those of fluorescein, but it has a higher quantum yield than FM.

The intrinsic fluorescence of the C317S or wild-type proteins was measured on an Amico Bowman (Los Angeles, CA) Series 2 spectrofluorimeter or a modified Photon Technologies Inc. (Monmouth Junction, NJ) Alphascan fluorimeter with excitation at 280 nm and emission integrated over 320−340 nm.

Data Analysis. To determine lifetimes, the luminescence data were fitted, using the Levenberg−Marquardt iteration method in Origin 7.0, to an exponential decay function

$$I(t) = B + \sum a_i \exp(-t/\tau_i) \qquad (1)$$

where $I(t)$ is the luminescence intensity at time t, B is the background count (usually determined to be zero), and a_i values are the pre-exponential factors for the components with τ_i lifetimes.

Fitting was performed by leaving out the first 100 μs of data to discriminate against signals arising from detector ringing or directly excited acceptor fluorescence decay. For samples labeled with only terbium donor, the data (at 490 nm) could be fitted very well (no systematic residuals) to two lifetimes. The origin of the shorter lifetime component, which varied from 2 to 10%, is unknown and could be due to either some quenched donor species in protein aggregates or a stereoisomer of the terbium chelate.

To determine the sensitized emission lifetime (at 520 nm), a small amount of leakage of the donor emission intensity through the acceptor filter was taken into account by making the following correction:

$$I'_{520DA}(t) = I_{520DA}(t) - \left[\frac{I_{520D}(t)}{I_{490D}(t)}\right] \times I_{490DA}(t) \qquad (2)$$

where $I'_{520DA}(t)$ is the corrected intensity at time t, $I_{520DA}(t)$ is the measured intensity for a donor−acceptor dual-labeled sample with the 520 nm filter, $I_{520D}(t)/I_{490D}(t)$ is the ratio of the donor-only intensity at 520 and 490 nm, and $I_{490DA}(t)$ is the intensity of donor−acceptor samples with the 490 nm filter (we assume no leakage of sensitized emission into the donor channel, based on the sharp cutoff of the 490 nm filter and the negligible FM emission at wavelengths of <500 nm).

These corrected sensitized emission data could be fitted to either two or three exponentials, with slightly better residuals and lower reduced χ^2 being obtained for three-exponential fits. For three-exponential fits, the smallest exponential was relatively small in both lifetime (≤80 μs) and relative amplitude (∼2−3%), but was not removed even when fitting after the first 150 μs. The likely source of this lifetime is either from detector ringing due to the high intensity of the (short-lived) acceptor fluorescence emission or from a very large energy transfer arising from aggregated protein molecules in the sample.

The presence of multiple components in the donor decay itself slightly complicates the interpretation of the various lifetimes. Here we have reported LRET distances by two different methods. In method I, we have used only the longest-lifetime components of the donor and acceptor emission decay fits to calculate the energy transfer efficiency (E). This is the customary method for determining LRET efficiencies and is calculated by

$$E = 1 - \frac{\tau_{AD}}{\tau_D} \qquad (3)$$

where τ_{AD} is the lifetime of the longest-lifetime component of the sensitized emission decay and τ_D is the corresponding longest-lifetime component of the donor decay.

In method II, we have calculated energy transfer efficiencies by weighted averaging of all the lifetime components. To do this, accurate values are needed for the amplitudes for each lifetime component, i.e., fraction of the donors having that lifetime. Usually this is given by

$$A_i = \frac{a_i\tau_i}{\sum a_i\tau_i} \qquad (4)$$

However, Heyduk and Heyduk (*27*) have shown that in LRET measurements, when the sensitized emission has multiple lifetimes, the amplitudes of the decay components do not accurately represent the relative prevalence of the corresponding donor species. This happens because the amplitude of each acceptor decay component depends linearly on the rate of energy transfer, in addition to the concentration of donors from which the energy transfer

Table 1: LRET Data for Wild-Type Recombinant Proteins[a]

		component (method I)				averaged (method II)			
pH	R_0	τ_D	τ_{AD}	ET %	R	τ_D	τ_{AD}	ET %	R
5	38.0	1.74 ± 0.04	0.62 ± 0.03	64.3 ± 1.2	34.9 ± 0.4	1.58 ± 0.06	0.57 ± 0.03	64.3 ± 0.6	34.3 ± 0.3
6	41.1	1.76 ± 0.05	0.46 ± 0.03	74.1 ± 1.2	34.9 ± 0.5	1.55 ± 0.10	0.42 ± 0.02	73.1 ± 0.5	34.5 ± 0.3
7	43.5	1.73 ± 0.02	0.41 ± 0.01	76.4 ± 0.9	36.1 ± 0.3	1.43 ± 0.02	0.36 ± 0.01	74.8 ± 0.5	35.5 ± 0.1
8	45.0	1.96 ± 0.04	0.49 ± 0.02	74.8 ± 1.1	38.7 ± 0.3	1.82 ± 0.09	0.39 ± 0.01	78.6 ± 1.6	36.8 ± 0.3
9	46.2	1.74 ± 0.03	0.57 ± 0.01	67.5 ± 0.2	41.4 ± 0.1	1.47 ± 0.06	0.47 ± 0.01	67.7 ± 1.0	40.2 ± 0.2
10	45.5	1.75 ± 0.02	0.81 ± 0.02	53.9 ± 1.3	45.0 ± 0.4	1.58 ± 0.09	0.67 ± 0.05	57.9 ± 1.3	43.0 ± 0.7

[a] Means ± the standard error of the mean of lifetimes, energy transfers (ET %), and distances (R) at each pH obtained either by taking the longest lifetime component (method I) or by using the lifetime averaging method (method II). For pH 5, 6, 8, and 10, $n = 4$, and for pH 7 and 9, $n = 3$. Note that the energy transfer and distance values are calculated pairwise for each experiment and then averaged.

occurs. Thus, a small population of donors which have very high efficiency for energy transfer to an acceptor will produce a large amplitude component in the sensitized acceptor decay.

Hence, instead of using the raw amplitudes obtained from eq 4, A_i, a correction is made in the relative amplitudes of the sensitized emission lifetimes based on the difference between the decay rates of the donor only and the corresponding donor component in the presence of acceptor.

$$A_i^{corr} = \frac{A_i/k_i}{\sum A_i/k_i}, \text{ where } k_i = \frac{1}{\tau_{ADi}} - \frac{1}{\tau_D} \quad (5)$$

where τ_D is the longest lifetime of the donor-only decay. After the correction, the population with the longest lifetime in the sensitized acceptor decay (τ_{AD}) is found to correspond in prevalence to the population with the longer donor lifetime (τ_D). Energy transfer efficiency (E) is calculated from the average lifetimes, using the following equation:

$$E = 1 - \frac{\langle \tau_{AD} \rangle}{\langle \tau_D \rangle} \quad (6)$$

The average lifetimes are defined by the equation

$$\langle \tau \rangle = \sum A_i \tau_i \quad (7)$$

where $A_i = A_i^{corr}$ for $\langle \tau_{AD} \rangle$.

In either method, donor−acceptor distances, R, are measured using the Förster equation:

$$R = R_0(E^{-1} - 1)^{1/6} \quad (8)$$

where the Förster distance, R_0, represents the distance at which the energy transfer efficiency is 50%.

$$R_0 = 0.211(\kappa^2 Q_d n^{-4} J]^{1/6} \text{ (in angstroms)} \quad (9)$$

where κ^2, the orientation factor, is taken to be $^2/_3$ (see Discussion below), Q_d is the donor quantum yield, n is the refractive index of the medium, and J is the spectral overlap (in M^{-1} cm^{-1} nm^4) defined as

$$J = \frac{\sum F_d(\lambda)\epsilon_a(\lambda)\lambda^4 \Delta\lambda}{\sum F_d(\lambda)\Delta\lambda} \quad (10)$$

Since the absorbance of the acceptor (ϵ_a), fluorescein maleimide (FM), varies with pH, the overlap integral J changes with pH. R_0 is also dependent on donor quantum yield Q_d. In the case of the terbium chelates, the quantum yield is calculated by comparing the measured donor lifetime to the known terbium lifetime (2.63 ms) in D_2O (where $Q_d = 1.0$) (*28*). Here, the R_0 values at the different pH's, as reported in Table 1, were determined by calculating the value of J for that pH and by assuming the quantum yield of the donor to be equal to 0.61 (when $\tau_D = 1.60$ ms). To take into account the variations in Q_d due to the variations in donor lifetime, the distances were calculated by the equation

$$R = R_0(E^{-1} - 1)^{1/6}\left(\frac{\tau_D}{1.6}\right)^{1/6} \quad (11)$$

Energy transfer efficiencies and the corresponding distances were calculated pairwise with τ_{AD} and τ_D values obtained from each experiment (each with a separate preparation of labeled protein) and then averaged to obtain the mean distances. Distances determined by using the longest lifetime components (method I) are described as "component", and those determined by using average lifetimes (method II) are described as "averaged" distances throughout the text. All lifetimes, energy transfer efficiencies, and distances are presented as means ± the standard error of the mean.

pH titration data for distances or intrinsic fluorescence were fitted using Origin 7.0 to either a two-step titration curve

$$y = \frac{A_1 \times 10^{2pH-pK_1-pK_2} + A_2 \times 10^{pH-pK_2} + A_3}{1 + 10^{2pH-pK_1-pK_2} + 10^{pH-pK_2}} \quad (12)$$

or a one-step titration curve

$$y = \frac{A_1 \times 10^{pH-pK_2} + A_2}{1 + 10^{pH-pK_2}} \quad (13)$$

where A_1−A_3 are the intrinsic fluorescence values or distances for the high-pH (H), intermediate-pH (I), and low-pH (L) forms of the protein, respectively.

RESULTS

The basic principle and the advantages of using luminescence energy transfer to measure the intermonomer distance between identical residues within a homodimer such as cdAE1 have been described in detail elsewhere (*26*, *29*). Briefly, by labeling cdAE1 dimers simultaneously with donor and acceptor labels, a heterogeneous population is generated that includes dimers labeled with only donors (DD) or only acceptors (AA), in addition to dimers labeled with a single donor and a single acceptor (DA). The terbium chelate

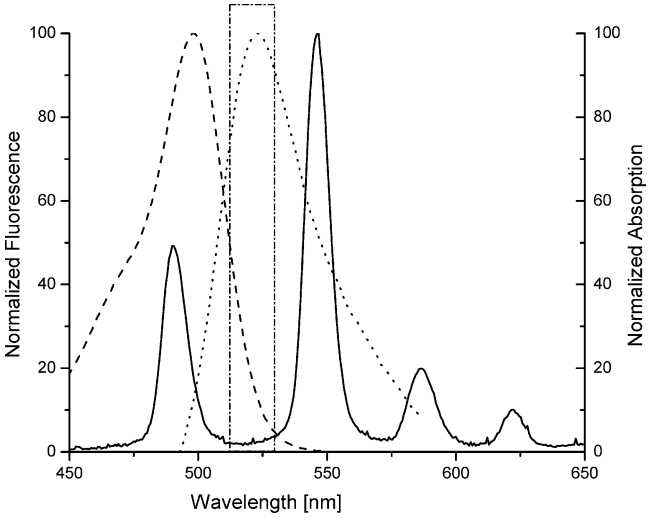

FIGURE 2: Emission and absorption spectra for the donor and acceptor used in LRET. The normalized emission spectrum of TbM (—) was measured by a CCD camera, with excitation by a 343 nm pulsed dye laser, and a delay of 100 μs after the laser pulse. Data were collected for 4 ms. Superimposed are the normalized absorption (- - -) and emission (•••) spectra of fluorescein maleimide, indicating good overlap between the terbium peak at 490 nm and fluorescein absorbance. Stimulated emission is detected with a 520 $\pm$ 5 nm filter (indicated by the rectangular box) that eliminates almost the entire donor signal except for a small bleed-through as mentioned in Experimental Procedures.

maleimide (TbM), which is used as the donor in LRET experiments, has a millisecond lifetime and a spiked luminescence emission profile (Figure 2) with a strong spectral overlap with the absorbance of the acceptor, fluorescein maleimide (FM), at 490 nm. On the other hand, TbM emission is almost negligible at the emission maximum of FM at 522 nm (Figure 2). Energy transfer in the DA species can be selectively assessed by recording the sensitized emission lifetime at the acceptor emission maximum wavelength, where the DD species will not contribute to any signals, using an appropriate filter (520 $\pm$ 10 nm, rectangular box in Figure 2). Direct excitation of the FM acceptors, greatly reduced by using ultraviolet light (337 nm), will generate fluorescence that decays in nanoseconds, while data acquisition does not begin until 100 μs after the excitation pulse. Hence, the AA species do not contribute to the signal. Therefore, by spectral and temporal discrimination, only dimers with a donor on one monomer and an acceptor on the adjacent monomer (DA species) contribute to sensitized emission at 520 nm. In the DA species, excited donors transfer energy to the acceptors gradually on the millisecond time scale, and each excited acceptor then immediately ($\tau \sim 4$ ns) emits fluorescence; therefore, the whole ensemble of the sensitized acceptor emission accurately reflects the decay rate of the DA species donors.

Labeling of Recombinant cdAE1 and IOVs. Figure 3 shows SDS−PAGE gels of the labeled proteins and IOVs viewed by either UV illumination or Coomassie staining. After purification with a Ni^{2+} column, the wild-type and C317S proteins were more than 95% pure, which is sufficient for the experiments since the impurities do not show any labeling (see lane 3 in Figure 3). In IOVs, the majority (~60−70%) of the total fluorescence is associated with the AE1 band (lane 1). Trypsin (lanes 2 and 5) digestion indicates that there is no fluorescence associated with the membrane domain [there are three cysteines in the membrane domain of hAE1, but all of them have been shown to be unreactive to maleimide (*30*)].

Conformational Transitions in cdAE1. The pH-induced conformational change in cdAE1 has been characterized mainly by observing changes in the intrinsic fluorescence or Stokes radius. This conformational change is thought to occur in two steps giving rise to low-pH (L), intermediate-pH (I), and high-pH (H) forms.

$$\mathrm{L} \underset{\mathrm{p}K_1}{\longleftrightarrow} \mathrm{I} \underset{\mathrm{p}K_2}{\longleftrightarrow} \mathrm{H}$$

Low and co-workers have reported values of 7.2 and 9.2 for pK_1 and pK_2, respectively (*21*), for cdAE1 purified from

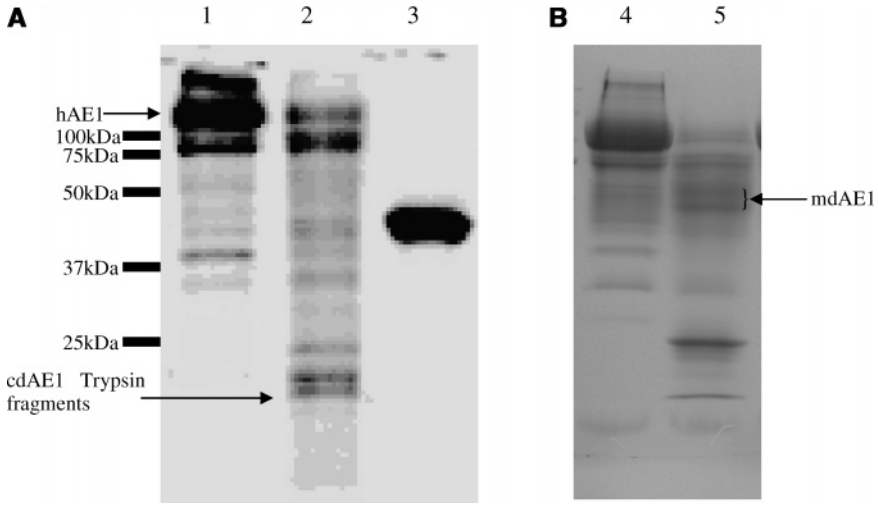

FIGURE 3: Labeling in IOVs and cdAE1. (A) Fluorescence gels showing labeling in IOVs (lane 1) and in wild-type cdAE1 (lane 3). Both IOVs and cdAE1 are labeled with a combination of TbM and FM as described in Experimental Procedures. The fluorescence signal from the hAE1 band is ~70% of the total IOV fluorescence. IOVs (1 mg/mL total protein) were digested with trypsin (50 μg/mL) for 30 min on ice. As shown in lane 2, there is almost no fluorescence intensity in the region where mdAE1 runs (~55 kDa). (B) Coomassie-stained gel showing IOVs (lane 4) and trypsin-digested IOVs (lane 5). The mdAE1 is visible as a diffuse band (marked with an arrow) in lane 5. Fluorescence gel images were captured with a Bio-Rad (Hercules, CA) FluoroMax imaging system using ultraviolet illumination and a 520 nm long-pass filter.

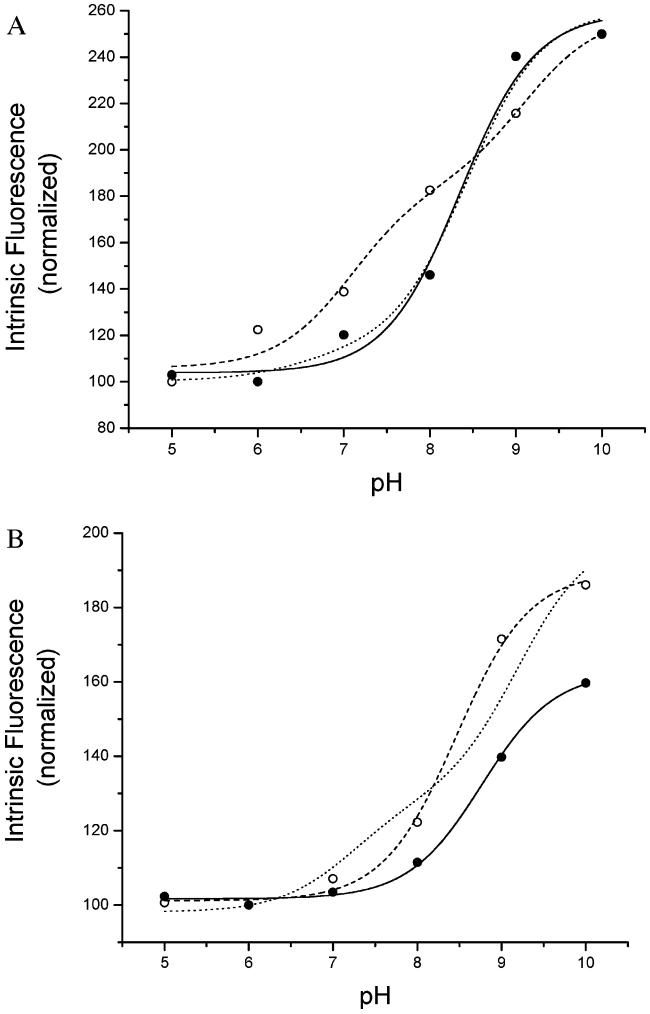

FIGURE 4: Intrinsic fluorescence of (A) wild-type and (B) C317S recombinant cdAE1 proteins that are either unlabeled (○) or labeled with FM (●), measured with excitation at 280 nm and emission integrated from 320 to 340 nm. In panel A, the wild-type unlabeled data can be fitted by eq 12 to give a pK_1 of 7.1 ± 0.5 and a pK_2 of 9.1 ± 0.7 (- - -). The best fit for the labeled wild type is shown by the solid line with a pK of 8.4 ± 0.1; the dotted line represents a two-titration fit of the labeled data which gives a pK_1 of 6.5 ± 4.5 and a pK_2 of 8.6 ± 0.5. In panel B, C317S unlabeled fits to a single titration with a pK of 8.5 ± 0.3 (- - -); the dotted line represents a forced two-titration fit in which pK_1 = 7.2 and pK_2 = 9.2, which were kept constant. The best fit for labeled C317S was obtained with a single titration with a pK of 8.8 ± 0.5 (—).

red blood cells via enzymatic cleavage. To determine if our recombinant cdAE1 proteins with $(His)_6$-tags undergo the same conformational changes, the intrinsic fluorescence of the unlabeled proteins, as well as proteins labeled with FM, was measured as a function of pH. The effect of TbM labeling on intrinsic fluorescence could not be measured, since the terbium chelate absorbs strongly around 280 nm and emits at 340 nm.

In the case of wild-type cdAE1 (Figure 4A), more than a doubling of the fluorescence is observed between pH 5 and 10, in both labeled and unlabeled proteins. For the unlabeled wild type (○), a double-titration curve can be fitted by eq 12 to obtain pK values of 7.1 ± 0.5 (L → I) and 9.1 ± 0.7 (I → H) (dashed line), which agree with the published values mentioned above. For the labeled protein (●), a two-titration curve (dotted line, pK_1 = 6.5 ± 4.5, pK_2 = 8.6 ± 0.5) can be fitted, but the error in pK_1 is very large. These data fit better to a single titration curve with eq 13 (χ^2 = 0.58 as compared to 1.38 for the two-titration fit) with a pK of 8.4 ± 0.1 (solid line). The effect of FM labeling on the behavior of the intrinsic fluorescence is similar to the observations reported by Low et al. (*21*) when cdAE1 sulfhydryl groups were reacted with iodoacetamide or glutathione, or cross-linked by oxidation.

In the case of the C317S protein (Figure 4B), the increase in intrinsic fluorescence in going from pH 5 to 10 is smaller than that observed for the wild type. Additionally, even for the unlabeled protein (○), the best fit to the fluorescence data is obtained by assuming a single titration (eq 13) with a pK of 8.5 ± 0.3 (dashed line). An attempt to fit the data to a two-titration curve by fixing the values of pK_1 and pK_2 to 7.2 and 9.2, respectively (dotted line), did not result in a good fit. For the labeled C317S (●), the best fit was again obtained by a single titration with a pK of 8.8 ± 0.5 (solid line). These observations indicate that the labeling of cdAE1 with maleimide probes and/or the mutation of Cys^{317} to a serine alters the structure of cdAE1 and its response to pH, at least as reported by the changes in intrinsic fluorescence. The fact that intrinsic fluorescence increases significantly with pH, however, provides evidence that the pH-induced conformational change is still taking place.

LRET Measurements and Effects of pH on Intermonomer Cys^{201} Distances in cdAE1. A typical data set of normalized luminescence emission decays for the labeled C317S protein at pH 8 and 10 is shown in Figure 5A (for clarity, data are shown for only two pH values). The donor-only decay curves are similar at both pH's (light blue and black). The donor−acceptor curves indicate that there is a strong quenching as a result of energy transfer, and show a decrease in lifetime at pH 8 (red) as compared to that at pH 10 (dark blue). This indicates that the inter-Cys^{201} distance is larger at pH 10, resulting in less energy transfer and hence a longer lifetime.

Figure 5B shows the dependence on pH of the calculated intermonomer distance between the Cys^{201} sites in C317S proteins as measured by LRET, using either the longest component (method I, black squares) or the averaged lifetimes (method II, red circles). There is only a small difference between the distances for averaged versus component data, and the trends are similar. There is no significant change in distance between pH 5 and 7 ($p > 0.05$), followed by a small but statistically significant ($p < 0.05$) increase at pH 8, relative to that at pH 5, and then a substantial increase up to pH 10 (see Table 2). The changes in distance were fitted with the pH titration (eqs 12 and 13), and the better fit was obtained with a single-pH titration curve, with a pK of 8.6 ± 0.1 for component distances (black line) and 8.8 ± 0.1 for averaged distances (red line), in good agreement with the pK (8.8 ± 0.5) obtained from intrinsic fluorescence (Figure 4B).

The dependence of component and averaged distances on pH for the wild-type protein is shown in Figure 5C, and the values are reported in Table 1. The pattern of conformational changes is somewhat different from that observed for C317S, with similar changes in distance occurring between pH 5 and 8 and between pH 8 and 10 (see Table 2). Again, component distances are slightly larger than the average distances, but they exhibit similar trends. Note that the distances measured in the wild-type protein (Figure 5C) are roughly equal to or slightly larger than the distances

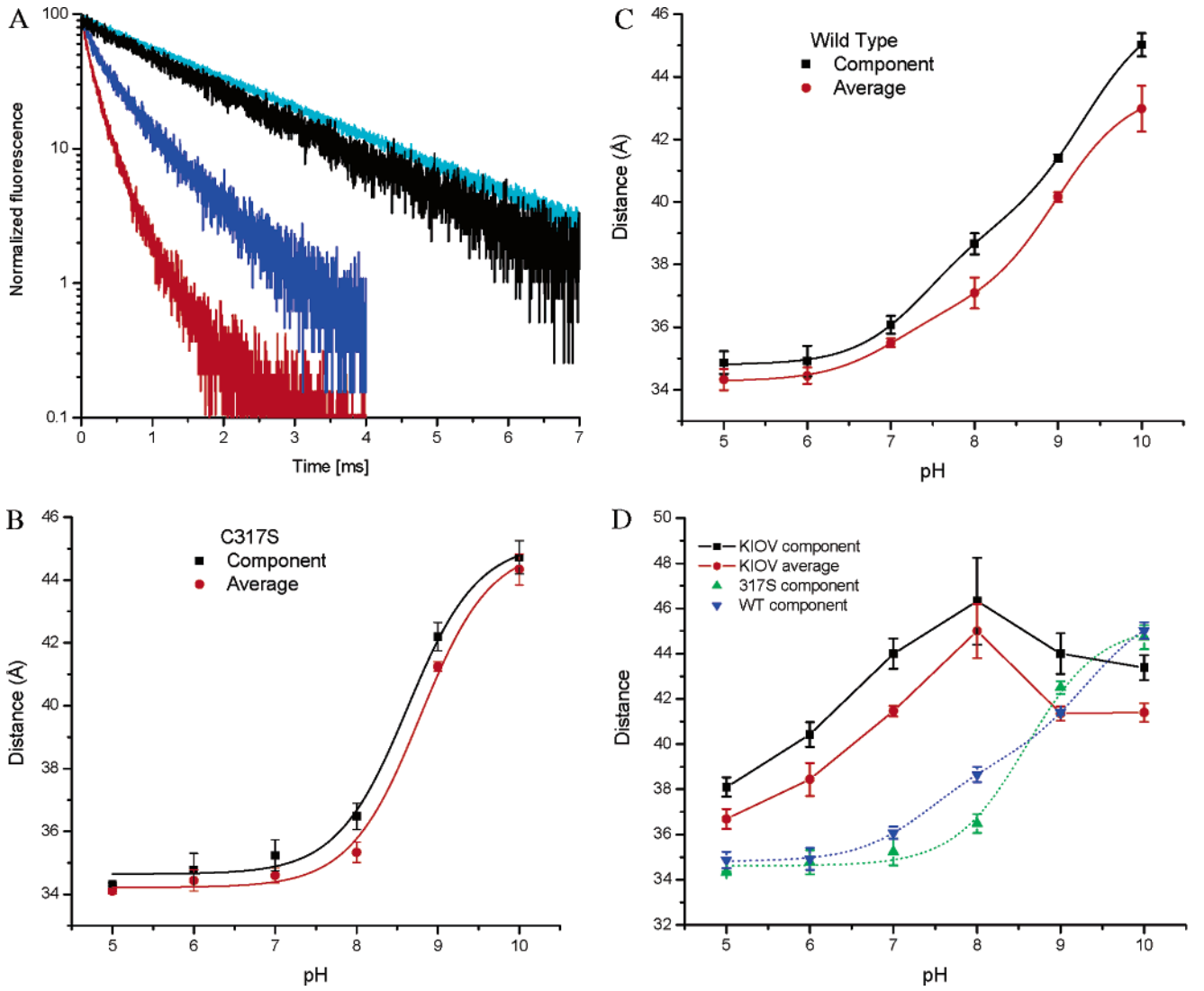

FIGURE 5: Inter-Cys^{201} distance measurements by LRET and effect of pH. (A) Typical data for normalized luminescence emission decay for donor-only and stimulated emission decay for donor- and acceptor-labeled 317S proteins in TB50 buffers at pH 8 and 10. The donor-only decays (light blue for pH 8 and black for pH 10) are similar. In the donor−acceptor samples, the sensitized emission (represented by red and blue for pH 8 and 10, respectively), representing the donor decay, has a shorter lifetime due to energy transfer. The lifetime is shorter at pH 8 than at pH 10, indicating that the inter-Cys^{201} distances are larger at pH 10. Samples were excited at 337 nm, and the emission was measured with appropriate filters. The first 100 μs of decay was ignored to discriminate against nanosecond lifetime fluorescence decay and detector ringing. (B−D) Plots of component (black squares and lines) or averaged (red circles and lines) inter-Cys^{201} LRET distance vs pH for (B) C317S cdAE1, (C) wild-type cdAE1, and (D) IOVs. Panel D also shows the component distances of C317S and wild-type cdAE1 in green and blue, respectively, for comparison.

Table 2: Distance Changes with pH[a]

	Δ(pH 5 → 8)	Δ(pH 8 → 10)	Δ(pH 5 → 10)
C317S	2.2 ± 0.4	8.2 ± 0.6	10.4 ± 0.5
wild type	4.3 ± 0.7	5.8 ± 0.7	10.1 ± 0.4
IOVs	8.2 ± 0.8	~0[b]	~8

[a] Changes in inter-Cys^{201} distances (in angstroms) occurring in C317S, wild type, and IOVs between pH 5 and 8 and between pH 8 and 10, as well as the total changes between pH 5 and 10. The difference between the component distances for each pair of pH values was calculated for each individual titration experiment. Values report the mean ± the standard error of the mean of all measurements ($n = 4$). [b] Difference between distances not statistically significant ($p > 0.05$) in this range (all other differences are significantly different).

measured in C317S (Figure 5B). If the cysteines at position 317 in the wild-type protein dimer were being labeled as well as Cys^{201}, there would be additional intermonomer and intramonomer energy transfer between the labels at positions 317 and 201. According to the crystal structure, the Cys^{317}−Cys^{201} intramonomer (30 Å) and intermonomer (25 Å) distances, as well as the Cys^{317} intermonomer (25 Å) distance, are smaller than the Cys^{201} intermonomer distance (42 Å). Hence, there would be higher energy transfer efficiency and consequently a much lower average measured distance if Cys^{317} were labeled, which is contrary to the experimental observations. This lack of Cys^{317} reactivity agrees with data indicating that *N*-ethylmaleimide labels preferentially at Cys^{201} in the wild-type protein (*20*). Moreover, when we attempted to label Cys^{317} by reacting the C201S mutant with TbM, no detectable labeling was observed (data not shown). The distance values in the wild-type protein are best fitted to two pH titrations with p*K*'s of 7.4 ± 0.1 and 9.3 ± 0.2 for the averaged distance (red line)

or 7.0 ± 0.1 and 9.0 ± 0.1 for the component distances (black line), comparable to the p*K*'s obtained from intrinsic fluorescence versus pH measurements in the unlabeled protein.

To calibrate the LRET measurements, the inter-Cys^{201} distance was measured in both the wild type and C317S at pH 4.8, the conditions under which the protein was crystallized. It was found that this does not differ significantly from the distance measured at pH 5. This distance (~33.4 Å) is smaller than the inter-Cys^{201} distance between the sulfur atoms of the Cys^{201} residues as reported in the crystal structure of cdAE1 (~42 Å). Because of the size of the chromophores and the length of the chemical linkers used for attachment to the Cys^{201} sulfur atoms, this shorter LRET distance is expected. Also, because of the strong distance dependence of energy transfer, the transfer efficiencies are biased toward the distance of closest approach of the probes, especially for luminescent probes with lifetimes in the millisecond range. Other workers have also reported an underestimation of distances in comparison to crystal structures when using LRET (*31*). This underestimation should not affect conclusions about the *changes* in distance caused by pH. It should also be noted that the temperature factors for this region of the protein, in the crystal structure, are high and residues 202−211 immediately following Cys^{201} are poorly defined, so there is some uncertainty in the value for the intermonomer distance calculated from the crystal coordinates.

Effect of pH on LRET Distances for Native cdAE1 in IOVs. One of the advantages of LRET is that accurate measurements can be made in IOVs where cdAE1 is still linked to mdAE1 and in its natural membrane environment. The recombinant proteins described above consist of amino acid residues up to position 379, but hydropathy analysis and chemical labeling indicate that the first transmembrane segment begins near amino acid residue 405 (*32*). Moreover, the positions of residues 357−379 were not resolved in the crystallographic studies. It is possible that the 48 amino acids (residues 357−404) of the membrane attachment region could influence the structural and conformational properties of the rest of the cytoplasmic domain.

As shown in Figure 5D, there are some remarkable differences in the inter-Cys^{201} LRET distances measured in IOVs as compared to isolated cdAE1. First, the distances at pH 5 are slightly larger than those measured in recombinant proteins (shown as green and blue triangles on the same graph). Second, there is an ~8 Å increase in distance between pH 5 and 8 (see Table 2), which is more than double the change occurring in the wild type or C317S over the same pH range. Finally, the distance does not change significantly ($p > 0.05$) above pH 8. This indicates that the linkage of the protein to the membrane can produce significant changes in the structural properties of cdAE1. Interestingly, the inter-Cys^{201} distance for IOVs at pH 8 is very similar to the distance for the recombinant proteins at pH 10. Thus, a possible interpretation of the data is that the L → I and I → H transitions take place at much lower pH values in the IOVs (see Figure 7 and the Discussion below).

The longer distances observed in IOVs could be due to some contribution from nonspecific labeling as observed in the fluorescence gels (Figure 3). However, since energy transfer is strongly distance dependent, being proportional to the inverse 6th power of distance, the nonspecific labeling in IOVs should not affect the accuracy of the distance measurements in cdAE1, unless there are nonspecific sites, labeled with donor and acceptor, that are located close enough to contribute to the sensitized emission.

We observe almost no sensitized emission after mild trypsin cleavage of either the labeled recombinant proteins or IOVs. The absence of sensitized emission in recombinant cdAE1 indicates that mild trypsin cleavage, which removes the N-terminal 21 kDa region (before Cys^{201}, the labeling site) of cdAE1, disrupts the structure of the remaining part of the protein and probably causes dissociation of the cdAE1 dimer. The sensitivity of energy transfer in IOVs to trypsin cleavage is consistent with the hypothesis that nearly all of the observed sensitized emission arises from cdAE1. It is, however, possible that trypsin cleavage also affects energy transfers occurring at the nonspecific labeling sites in IOVs.

To further evaluate the possible effects of nonspecific labeling on the measured distances, sensitized emission data from IOVs were simulated assuming a worst-case scenario where the level of nonspecific labeling is 40% (the maximum observed) and all of these nonspecific sites contribute to the sensitized emission signal. Since the observed distances were longer in IOVs than in recombinant cdAE1, only cases in which the nonspecific donor−acceptor distance and, hence, sensitized lifetimes are larger than that measured in wild-type cdAE1 were considered. The simulated data, generated by assuming that 60% of the donors had the same τ value as that for isolated wild-type cdAE1 and the rest had a longer τ value (and corresponding smaller amplitude), were fitted to eq 1 with a single-exponential decay component to calculate the apparent lifetime and distance. The maximum deviation of this apparent distance from the cdAE1 distance in the simulations was only 1.8 Å, and occurred when the nonspecific lifetime was assumed to be ~1.75 times the specific lifetime.

Even the largest possible increase in the apparent distance (1.8 Å) calculated by the simulation is smaller than the observed 3 Å difference between IOVs and pure recombinant proteins at pH 5. At higher pH's, the difference in distance is even greater (~8 Å), so it is highly unlikely that the nonspecific labeling could explain the increased inter-Cys^{201} distance at pH ≤8 observed in IOVs. Moreover, it is quite improbable that the nonspecific contribution could be as high as assumed in the simulation. Together with the trypsin cleavage results, these calculations provide evidence that the different pH-dependent conformational behavior in IOVs is not due to nonspecific labeling, but instead represents an effect of the attachment of cdAE1 to the membrane domain.

Effects of Enzyme Binding, Ionic Strength, and Nature of Anion. A number of important cytosolic proteins are associated with cdAE1 through the PPB domain, particularly ankyrin, hemoglobin, and the glycolytic enzyme glyceraldehyde-3-phosphate dehydrogenase (G3PDH). Since there is evidence that binding of some of these peripheral proteins can affect the conformation of cdAE1 (*22*), it would be worthwhile to determine their effects on the inter-Cys^{201} distance. Unfortunately, the binding of ankyrin is known to be inhibited by chemical modification of the sulfhydryl residues (*33*), and hemoglobin causes a quenching of the

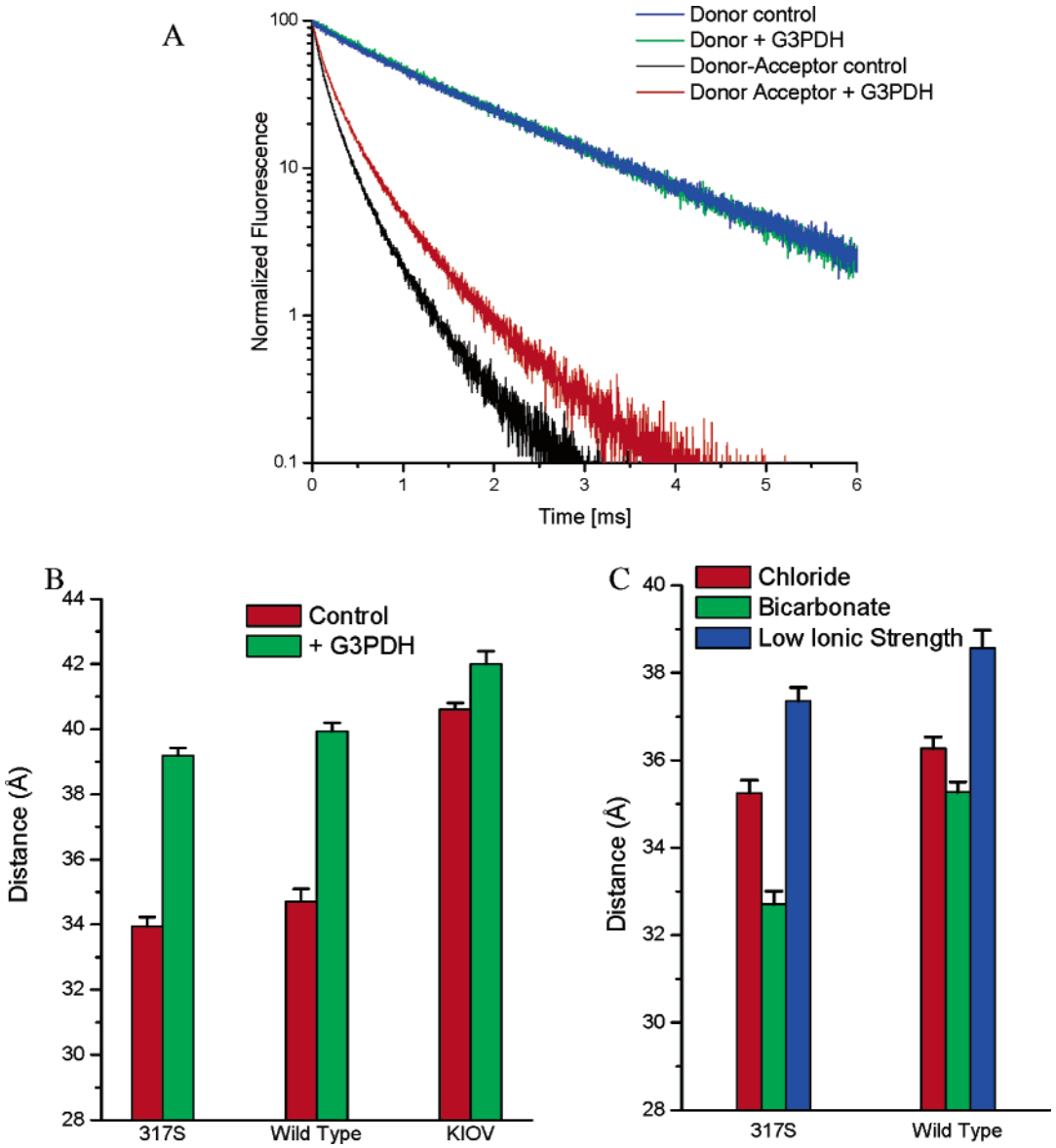

FIGURE 6: Effects of G3PDH and anions on the inter-Cys^{201} distance. (A) Effect of binding of G3PDH on the normalized donor decay or donor- and acceptor-sensitized emission for the C317S protein. (B) Summary of the effects of G3PDH on the inter-Cys^{201} distances (n = 3). (C) Effects of different ions and ionic strengths on the inter-Cys^{201} distance (n = 3). All differences are statistically significant (p < 0.05).

donor emission when bound to labeled cdAE1. However, it was possible to examine the effects of G3PDH binding on the inter-Cys^{201} distance.

Figure 6A shows the effect of binding of G3PDH on the donor and donor−acceptor luminescence decay curves for the C317S protein, labeled with TbM and Oregon Green (an acceptor similar to FM but with a higher quantum yield). The donor signal does not change significantly upon addition of G3PDH, but the lifetime of the sensitized acceptor emission increases dramatically (red curve) compared to controls, where only the buffer is added (black curve). From the results summarized in Figure 6B, it is observed that G3PDH binding at pH 6.5 causes the protein to adopt a more extended conformation, with an ~5 Å larger inter-Cys^{201} distance. Similar increases are observed in the wild-type protein, while the increases in lifetime and therefore in intermonomer distance are much smaller in IOVs, but still statistically significant. The latter observation agrees with the idea that cdAE1 is already in a more extended conformational state in IOVs, even at pH 6.5, and hence G3PDH binding does not have an effect equal to that in the recombinant proteins.

We have also investigated whether the substrates for the hAE1 anion exchanger, chloride and bicarbonate, have different effects on the structure of the cytoplasmic domain of the protein. Figure 6C summarizes the effect of Cl^- or HCO_3^-, as well as low ionic strength (all at pH 7.5), on the inter-Cys^{201} distances in wild-type and C317S proteins. The following buffers were used for the various conditions: chloride [150 mM KCl and 20 mM HEPES (pH 7.5)], bicarbonate [150 mM $KHCO_3$ and 20 mM HEPES (pH 7.5)], and low ionic strength (5 mM potassium phosphate). We observe a small but statistically significant (p < 0.05) decrease in the intermonomer distance when chloride ions are replaced with bicarbonate ions as well as a small increase (p < 0.05) in distance in a low-ionic strength buffer relative to that in Cl^- or HCO_3^- buffers. While the effect of the different anions further emphasizes the lability of the cdAE1

structure, the physiological relevance of this finding is uncertain, since extremely nonphysiological ionic concentrations (only bicarbonate vs only chloride) were used.

DISCUSSION

Reliability of Measurements. The LRET technique has provided the first direct information indicating a specific molecular conformational change in cdAE1 by enabling us to measure the intermonomer distance between fluorescent labels covalently attached to Cys^{201} in the cdAE1 protein, and to determine the effects of pH, ions, and ligand binding on this distance. LRET has been used successfully as a very sensitive tool for the determination of distance and change in distance in a variety of proteins and nucleic acids (*31*, *34*−*37*). For example, it has been successful in detecting motions as small as 1−2 Å in the Shaker K^+ channel (*38*). The reliability of LRET is enhanced by the fact that the orientation factor, κ^2 (in eq 9), is less uncertain than traditional fluorescence energy transfer with organic dye molecules, because the terbium ion is inherently depolarized (*39*). Previous reports have shown that FM covalently attached to Cys^{201} has some residual anisotropy, but still exhibits rotational freedom within a "cone angle" of ∼52°, and that the rotational lifetime of the labeled FM in its binding pocket is pH-independent (*20*). Moreover, since the signals are being measured over millisecond time scales, the probes have enough time to randomize. This makes the assumption of $\kappa^2 = {}^2/_3$, based on the random orientation of the donor and acceptor transition dipoles, much more accurate. Therefore, even though the absolute distance between the labeled cysteines is systematically underestimated due to the finite size and linkage of the fluorophores, changes in distance and comparisons of distances can be reliably interpreted.

Conformational Changes. Zhou and Low (*19*) hypothesized that the pH-induced conformational change might involve a movement of the PPB domain away from the dimerization domain around a hinge at Gly^{305} (Figure 1). This hypothesis was based on site-directed mutagenesis studies in which a putative hydrogen bond, formed between Trp^{105} in the PPB domain and Asp^{316} in the dimerization domain of the adjacent monomer, was disrupted. Mutation of either residue was found to affect the intrinsic fluorescence polarization and resistance to either thermal or urea denaturation at pH 6 and not at pH 10.5. This indicated that the hydrogen bond was being formed at the lower pH, but ruptured at the higher pH, consistent with the proposed movement of the PPB domain. Since Cys^{201} is located in the PPB domain, our distance versus pH measurements in wild-type and C317S recombinant proteins provide direct structural support for this hypothesis. However, other models, involving movement around a different hinge or even multiple hinges, are not ruled out by our data.

Although our data support the idea that cdAE1 adopts a more extended conformation at higher pH values, there are differences in the pH dependence of the inter-Cys^{201} distance for wild-type cdAE1 and the C317S mutant that require explanation. The LRET data for wild-type cdAE1 (Figure 5C) are best fit with a two-titration model, with p*K* values in agreement with those reported by Low and co-workers on the basis of changes in intrinsic fluorescence and Stokes radius. Thus, these data support the concept of a biphasic change in conformation, from an L state at low pH to an intermediate (I) state and then to a high-pH (H) state (Figure 7). Although there is clear LRET evidence for a two-step titration model for labeled wild-type cdAE1 (Figure 5B), the intrinsic fluorescence data (Figure 4A) fail to show this. This indicates a limitation in the ability of the intrinsic fluorescence to detect conformational changes.

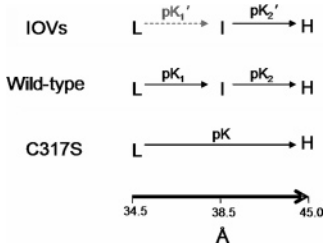

FIGURE 7: Proposed mechanism for pH-dependent conformational changes in wild-type cdAE1, C317S cdAE1, and cdAE1 in IOVs.

Surprisingly, for the C317S mutant, both the dependence of the inter-Cys^{201} distance (Figure 5B) and the dependence of the intrinsic fluorescence (Figure 4B) on pH fit very well to a single-titration model. Furthermore, the good agreement of the distance values at the two ends of the pH range that was tested, pH 5 and 10 (see Table 2), indicates that the same overall change in distance occurs for the wild-type and C317S proteins. The simplest explanation for this behavior is that for the C317S mutant, the conformational change from L to H occurs in one step (Figure 7), with a high p*K* value similar to pK_2 for the wild-type transition from I to H. That is, changes in pH in the range of 5−8 do not cause a significant appearance of the I conformation in the C317S mutant.

The somewhat smaller changes in intrinsic fluorescence observed for C317S as compared to those for the wild type indicate that there are subtle differences in the overall structure of the mutant and wild type, as expected, but do not contradict the clear evidence from the LRET measurements for a similar change in conformation of the region containing Cys^{201}. Although it would be premature to speculate on the reason for the alteration of the pH-dependent behavior in C317S, the fact that a conservative mutation has such a large effect provides further evidence for the conformational flexibility of cdAE1.

In IOVs, it is proposed (Figure 7) that the p*K*'s for the conformational transitions are drastically reduced such that the L → I change has already taken place at pH 5 (or cdAE1 is in a somewhat altered L′ or I′ form) and that the increase in LRET distance between pH 5 and 8 represents the I → H transition occurring at a lower pH (with a lower pK_2 value, pK_2'). The fact that the LRET distance increases to the same value by pH 8 in IOVs that it reaches by pH 10 in isolated cdAE1 (wild-type or C317S) indicates that the IOV cdAE1 at pH 8 is indistinguishable from the isolated cdAE1 at pH 10 in terms of the inter-Cys^{201} distance. In both cases, cdAE1 is in the H (high-pH) conformation (Figure 7).

The remarkably altered conformational transition profile in IOVs indicates a substantial effect of the linkage between the membrane and the cytoplasmic domain of hAE1 on the structure of the latter. This effect could be due to the covalent linkage of cdAE1 to the membrane domain of the protein and/or due to noncovalent interactions between the two

domains. Since inter-Cys^{201} distances at physiological pH are much larger in IOVs than in recombinant cdAE1, it indicates that the physiological structure of cdAE1 is different from the structure of cdAE1 at the same pH and also different from the crystal structure obtained at pH 4.8 (using recombinant cdAE1), with the protein adopting a more extended conformation when linked to the membrane. The effect of this linkage on cdAE1 conformation has been observed previously. Thevenin et al. have reported a much steeper increase in the level of pH-dependent segmental motion of cdAE1 at the Cys^{201} region in IOVs as compared to that in the isolated cdAE1 obtained by chymotryptic cleavage (*20*). Additionally, Southeast Asian ovalocytosis, a hAE1-related disease, is caused by a mutation where nine amino acid residues (400−408) at the boundary of the cytoplasmic and membrane domains are absent. This disease is characterized by increased cell rigidity caused by a conformationally altered cdAE1 becoming entangled in the cytoskeletal protein network through nonspecific interactions (*40*). This suggests that the small membrane-proximal region (amino acids 400−408) has a large effect on the global conformation of cdAE1.

It could be possible that the difference in the sensitivity of the cytosolic domain to pH in IOVs is due to local differences in pH or ion composition near the membrane surface. However, in view of the relatively high ionic strength at which the experiments were carried out, which should minimize any effects of fixed charges on the proton or ion distribution near the surface, this would be unlikely. To explain the effect, the pH would have to be higher near the membrane interface in the IOVs; that is, the proton concentration would be lower. To obtain the major shift in p*K* that occurs, a very high concentration of local positive charge would be required. Although topological models predict that some of the cytoplasmic loops of hAE1 are rich in positive charges (*1*), these would be neutralized by the negatively charged phosphatidyl serine in the inner leaflet of the bilayer.

Physiological Significance. The physiological significance of the observed pH-induced changes in purified cdAE1 has been somewhat of a mystery, since the internal pH of red blood cells is not expected to vary greatly. However, as demonstrated here, the conformation of the cdAE1 dimer is quite flexible even without pH changes. Thus, it is observed that the linkage of cdAE1 to the membrane through the C-terminal region results in a more extended conformation even at physiological pH. At the other end of cdAE1, the binding of a glycolytic enzyme, G3PDH, to the flexible N-terminal segment (*41*, *42*) also causes the protein to adopt a more extended conformation even at a low pH.

Conformational effects of pH and protein binding have been reported by other groups, as well. For example, light scattering experiments have shown that binding of hemoglobin to cdAE1 affects its conformation (*12*). Ankyrin, important for membrane−cytoskeleton linkage, has been shown to bind more avidly to the low-pH conformation of the protein (*15*, *33*). Interestingly, the effect of G3PDH on cdAE1 conformation seems to be the opposite of that of ankyrin. Additionally, it has been shown that binding of ankyrin affects the binding of protein 4.1 at the N-terminal tail of cdAE1 (*43*), where G3PDH is proposed to bind. Hence, it is possible that the pH-dependent conformational flexibility of cdAE1 actually reflects a metastable equilibrium between its various forms at physiological pH that allows it to quickly regulate red blood cell shape and metabolism through modulation of the binding and debinding of various peripheral proteins. Observations made on single cdAE1 dimers using single-pair FRET (*44*), a method that can reveal low-probability conformational states hidden in ensemble measurements, indicate that the protein may adopt multiple conformations at physiological pH.

Conclusions. We have demonstrated that it is possible by using LRET to measure the intermonomer distance between identical residues within the cdAE1 dimer and determine how the distance changes with pH and other factors. It should be possible to extend this technique to cdAE1 mutants containing unique cysteine residues in other parts of the protein to test our hypothesis regarding the different conformational changes in wild-type and C317S cdAE1 and cdAE1 in IOVs and to develop a more complete map of the molecular conformational changes occurring in cdAE1 in response to pH or protein binding. In particular, we have not been able to investigate the effect of ankyrin on the intermonomer distances, since derivatization of the Cys^{201} residue with sulfhydryl reagents causes a loss of ankyrin binding. It should be possible to observe the ankyrin binding effects by engineering unique cysteines at different sites.

ACKNOWLEDGMENT

We thank Drs. Philip Low and Jianzhong Zhou, Purdue University, for the generous gift of the wild-type and C317S plasmids; Todd Ryder and Dr. Robert Boeckman, University of Rochester, for the synthesis of terbium chelates; and Dr. Paul Selvin, University of Illinois, Urbana, IL, for helpful advice on the purchase and setup of equipment for luminescence lifetime measurements.

REFERENCES

1. Knauf, P. A., and Pal, P. (2003) in *Red Cell Membrane Transport in Health and Disease* (Bernhardt, I., and Ellory, J. C., Eds.) pp 253−301, Springer, Berlin.
2. Low, P. S. (1986) Structure and function of the cytoplasmic domain of band 3: Center of erythrocyte membrane-peripheral protein interactions, *Biochim. Biophys. Acta 864*, 145−167.
3. Zhang, D., Kiyatkin, A., Bolin, J. T., and Low, P. S. (2000) Crystallographic structure and functional interpretation of the cytoplasmic domain of erythrocyte membrane band 3, *Blood 96*, 2925−2933.
4. Chang, S. H., and Low, P. S. (2003) Identification of a critical ankyrin-binding loop on the cytoplasmic domain of erythrocyte membrane band 3 by crystal structure analysis and site-directed mutagenesis, *J. Biol. Chem. 278*, 6879−6884.
5. Bennett, V., and Stenbuck, P. J. (1980) Association between ankyrin and the cytoplasmic domain of band 3 isolated from T erthrocyte membrane, *J. Biol. Chem. 255*, 6424−6432.
6. An, X. L., Takakuwa, Y., Nunomura, W., Manno, S., and Mohandas, N. (1996) Modulation of band 3-ankyrin interaction by protein 4.1. Functional implications in regulation of erythrocyte membrane mechanical properties, *J. Biol. Chem. 271*, 33187−33191.
7. Korsgren, C., and Cohen, C. M. (1988) Associations of human erythrocyte band 4.2. Binding to ankyrin and to the cytoplasmic domain of band 3, *J. Biol. Chem. 263*, 10212−10218.
8. Murthy, S. N. P., Liu, T., Kaul, R. K., Kohler, H., and Steck, T. L. (1981) The aldose-binding site of the human erythrocyte membrane is at the NH_2 terminus, *J. Biol. Chem. 256*, 11203−11208.
9. Low, P. S., Rathinavelu, P., and Harrison, M. L. (1993) Regulation of glycolysis via reversible enzyme binding to the membrane protein, band 3, *J. Biol. Chem. 268*, 14627−14631.

10. Tsai, I., Murthy, S. N. P., and Steck, T. L. (1982) Effect of red cell membrane binding on the catalytic activity of glyceraldehyde-3-phosphate dehydrogenase, *J. Biol. Chem. 257*, 1438−1442.
11. Jenkins, J. D., Kezdy, F. J., and Steck, T. L. (1985) Mode of interaction of phosphofructokinase with the erythrocyte membrane, *J. Biol. Chem. 260*, 10426−10433.
12. Salhany, J. M., Cordes, K. A., and Sloan, R. L. (1998) Characterization of the pH dependence of hemoglobin binding to band 3. Evidence for a pH-dependent conformational change within the hemoglobin-band 3 complex, *Biochim. Biophys. Acta 1371*, 107−113.
13. Waugh, S. M., and Low, P. S. (1985) Hemichrome binding to band 3: Nucleation of Heinz bodies on the erythrocyte membrane, *Biochemistry 24*, 34−39.
14. Harrison, M. L., Isaacson, C. C., Burg, D. L., Geahlen, R. L., and Low, P. S. (1994) Phosphorylation of human erythrocyte band 3 by endogenous p72syk, *J. Biol. Chem. 269*, 955−959.
15. Low, P. S., Willardson, B. M., Mohandas, N., Rossi, M., and Shohet, S. B. (1991) Contribution of the band 3-ankyrin interaction to erythrocyte membrane mechanical stability, *Blood 77*, 1581−1586.
16. Peters, L. L., Shivdasani, R. A., Liu, S. C., Hanspal, M., John, K. M., Gonzalez, J. M., Brugnara, C., Gwynn, B., Mohandas, N., Alper, S. L., Orkin, S. H., and Lux, S. E. (1996) Anion exchanger 1 (band 3) is required to prevent erythrocyte membrane surface loss but not to form the membrane skeleton, *Cell 86*, 917−927.
17. Southgate, C. D., Chishti, A. H., Mitchell, B., Yi, S. J., and Palek, J. (1996) Targeted disruption of the murine erythroid band 3 gene results in spherocytosis and severe haemolytic anaemia despite a normal membrane skeleton, *Nat. Genet. 14* (2), 227−230.
18. Kannan, R., Yuan, J., and Low, P. S. (1991) Isolation and partial characterization of antibody- and globin-enriched complexes from membranes of dense human erythrocytes, *Biochem. J. 278* (Part 1), 57−62.
19. Zhou, J., and Low, P. S. (2001) Characterization of the reversible conformational equilibrium in the cytoplasmic domain of human erythrocyte membrane band 3, *J. Biol. Chem. 276*, 38147−38151.
20. Thevenin, B. J., Periasamy, N., Shohet, S. B., and Verkman, A. S. (1994) Segmental dynamics of the cytoplasmic domain of erythrocyte band 3 determined by time-resolved fluorescence anisotropy: sensitivity to pH and ligand binding, *Proc. Natl. Acad. Sci. U.S.A. 91*, 1741−1745.
21. Low, P. S., Westfall, M. A., Allen, D. P., and Appell, K. C. (1984) Characterization of the reversible conformational equilibrium of the cytoplasmic domain of erythrocyte membrane band 3, *J. Biol. Chem. 259*, 13070−13076.
22. Thevenin, B. J., and Low, P. S. (1990) Kinetics and regulation of the ankyrin-band 3 interaction of the human red blood cell membrane, *J. Biol. Chem. 265*, 16166−16172.
23. Thevenin, B. J., Bicknese, S. E., Verkman, A. S., and Shohet, S. B. (1996) Distance between Cys-201 in erythrocyte band 3 and the bilayer measured by single-photon radioluminescence, *Biophys. J. 71*, 2645−2655.
24. Chen, J., and Selvin, P. R. (1999) Thiol-reactive luminescent chelates of terbium and europium, *Bioconjugate Chem. 10*, 311−315.
25. Bennett, V. (1983) Proteins involved in membrane-cytoskeleton association in human erythrocytes: Spectrin, ankyrin, and band 3, *Methods Enzymol. 96*, 313−324.
26. Knauf, P. A., and Pal, P. (2004) Use of luminescence resonance energy transfer to measure distances in the AE1 anion exchange protein dimer, *Blood Cells Mol. Dis. 32*, 360−365.
27. Heyduk, T., and Heyduk, E. (2001) Luminescence energy transfer with lanthanide chelates: Interpretation of sensitized acceptor decay amplitudes, *Anal. Biochem. 289*, 60−67.
28. Selvin, P. R. (2002) Principles and biophysical applications of lanthanide-based probes, *Annu. Rev. Biophys. Biomol. Struct. 31*, 275−302.
29. Selvin, P. R. (1996) Lanthanide-based resonance energy transfer, *IEEE J. Sel. Top. Quantum Electron. 2*, 1077−1087.
30. Rao, A. (1979) Disposition of the band 3 polypeptide in the human erythrocyte membrane, *J. Biol. Chem. 254*, 3503−3511.
31. Chen, Y., and Lehrer, S. S. (2004) Distances between tropomyosin sites across the muscle thin filament using luminescence resonance energy transfer: Evidence for tropomyosin flexibility, *Biochemistry 43*, 11491−11499.
32. Popov, M., Tam, L. Y., Li, J., and Reithmeier, R. A. F. (1997) Mapping the ends of transmembrane segments in a polytopic membrane protein. Scanning N-glycosylation mutagenesis of extracytosolic loops in the anion exchanger, band 3, *J. Biol. Chem. 272*, 18325−18332.
33. Thevenin, B. J., Willardson, B. M., and Low, P. S. (1989) The redox state of cysteines 201 and 317 of the erythrocyte anion exchanger is critical for ankyrin binding, *J. Biol. Chem. 264*, 15886−15892.
34. Burmeister, G. E., Cooke, R., and Selvin, P. R. (1998) Luminescence resonance energy transfer measurements in myosin, *Biophys. J. 74*, 2451−2458.
35. Chakrabarty, T., Yengo, C., Baldacchino, C., Chen, L. Q., Sweeney, H. L., and Selvin, P. R. (2003) Does the S2 rod of myosin II uncoil upon two-headed binding to actin? A leucine-zippered HMM study, *Biochemistry 42*, 12886−12892.
36. Heyduk, E., and Heyduk, T. (1999) Architecture of a complex between the σ70 subunit of *Escherichia coli* RNA polymerase and the nontemplate strand oligonucleotide. Luminescence resonance energy transfer study, *J. Biol. Chem. 274*, 3315−3322.
37. Chakrabarty, T., Xiao, M., Cooke, R., and Selvin, P. R. (2002) Holding two heads together: Stability of the myosin II rod measured by resonance energy transfer between the heads, *Proc. Natl. Acad. Sci. U.S.A. 99*, 6011−6016.
38. Cha, A., Snyder, G. E., Selvin, P. R., and Bezanilla, F. (1999) Atomic scale movement of the voltage-sensing region in a potassium channel measured via spectroscopy, *Nature 402*, 809−813.
39. Reifenberger, J. G., Snyder, G. E., Baym, G., and Selvin, P. R. (2003) Emission polarization of europium and terbium chelates, *J. Phys. Chem. B 107*, 12862−12873.
40. Mohandas, N., Winardi, R., Knowles, D., Leung, A., Parra, M., George, E., Conboy, J., and Chasis, J. (1992) Molecular basis for membrane rigidity of hereditary ovalocytosis. A novel mechanism involving the cytoplasmic domain of band 3, *J. Clin. Invest. 89*, 686−692.
41. Schneider, M. L., and Post, C. B. (1995) Solution structure of a band 3 peptide inhibitor bound to aldolase: A proposed mechanism for regulating binding by tyrosine phosphorylation, *Biochemistry 34*, 16574−16584.
42. Walder, J. A., Chatterjee, R., Steck, T. L., Low, P. S., Musso, G. F., Kaiser, E. T., Rogers, P. H., and Arnone, A. (1984) The interaction of hemoglobin with the cytoplasmic domain of band 3 of the human erythrocyte membrane, *J. Biol. Chem. 259*, 10238−10246.
43. Lombardo, C. R., Willardson, B. M., and Low, P. S. (1992) Localization of the protein 4.1-binding site on the cytoplasmic domain of erythrocyte membrane band 3, *J. Biol. Chem. 267*, 9540−9546.
44. Pal, P., Lesoine, J. F., Lieb, M. A., Novotny, L., and Knauf, P. A. (2005) A novel immobilization method for single protein spFRET studies, *Biophys. J. 89*, L11−L13.

BI0506831